

## RESEARCH ARTICLE

# Hydrodynamic Analysis of Integrated Interceptor-Stern Flap for Trim Control on High-Speed Planing Vessel

S. Samuel<sup>1\*</sup>, A. Supriyatin<sup>1</sup>, Dedy Chrismianto<sup>1</sup>, A.F. Zakki<sup>1</sup> and Dian Purnama Sari<sup>2</sup><sup>1</sup>Department of Naval Architecture, Faculty of Engineering, University of Diponegoro, Semarang 50275, Indonesia<sup>2</sup>Research Center for Hydrodynamics Technology, National Research and Innovation Agency (BRIN), Surabaya 60117, Indonesia

**ABSTRACT** – In a planing vessel, an interceptor is used to exercise control trim at a limited speed, which can result in excessive drag and bow trim at high speed. Previous studies have combined interceptors with stern flaps to achieve optimal hydrodynamic performance on planing hulls. This study investigated the hydrodynamic characteristics of a planing hull with an integrated interceptor-stern flap. The integrated interceptor-stern flap is a form of integration between the interceptor, which is mounted downwards and vertically on the transom, and the stern flap at the end. At high speed, the same interceptor (i) height converted to an integrated interceptor-stern flap can produce better results. Different flap angles were considered to affect interceptor performance. The fluid flow around the ship model was solved using the Reynolds-Average Navier-Stokes equation and the realizable k-epsilon turbulence model technique. The total number of meshes was determined using mesh independence. In conclusion, while the interceptor showcased significant reductions in resistance and trim across various Froude numbers, its effectiveness was compromised at high speeds due to increased drag and trim height, necessitating caution in its application. Furthermore, integrating stern flaps with the interceptor, particularly with a 5° angle, proved promising in further reducing drag and trim, highlighting the importance of interceptor design considerations for enhancing ship performance.

**ARTICLE HISTORY**

Received : 24<sup>th</sup> June 2023  
Revised : 11<sup>th</sup> Jan. 2024  
Accepted : 04<sup>th</sup> Apr. 2024  
Published : 20<sup>th</sup> June 2024

**KEYWORDS**

*Resistance*  
*Interceptor*  
*Stern flap*  
*Planing hull*  
*Interceptor-stern flap*

## 1.0 INTRODUCTION

Planing-type ships are unique because the design has a smaller hydrostatic force than the hydrodynamic force. This is the reason predicting the resistance of planing ships is more intricate compared to displacement hull types. The complexity is associated with the drag component in planing hull type influenced by the standard factors as well as trim (along the y-axis) and heave (along the z-axis) movements. Moreover, ship resistance is related to the speed which is normally influenced by the fluid force moving against the direction of motion. The reduction in the resistance normally leads to a decrease in the power released, thereby improving the performance of ships and reducing fuel consumption. It is also possible to add an appendage such as a stern wedge [1], extended stern [2], stern flap [3], hull vane [4], or interceptor [5], to the stern of the ship as an alternative to reduce resistance.

The stern flap is in the form of a short plate extending backward and generally oriented at a certain angle while the interceptor is a flat plate that moves vertically downwards to a certain depth from the stern of the ship [6]. Resistance can be reduced by fixing the stern flap to determine the relationship between changes in pressure distribution and waves on the transom [7] and the flow field of the ship to enhance the propulsion performance [8]. Zhou et al. used the stern flap to reduce resistance which potentially led to energy savings of 3–5% [9]. Another study by Zou et al. also simulated high-speed planing hull ships at flap angles of 2°, 3°, and 4.5° with the flow field observed to be in line with the experimental results [3].

Ghassemi and Mansoori [10] studied the impact of the interceptor on the hydrodynamic performance of fast boats to determine the ideal geometric parameters. The results showed that the interceptor caused intense pressure at the point of contact, leading to the reduction of the ship's wet surface and coefficient of friction. For the first time, the effect of boundary layer thickness on interceptor efficiency was investigated [5], [11], and the results proved the need to consider several parameters for excellent interceptor efficiency in addition to the height. However, the most important factor identified was the boundary layer which was abbreviated as the d/h ratio. The observation from the study further showed the ability of the interceptor to control porpoising instability [12].

Several studies reported that the installation of interceptors reduced resistance on cruise ships [13], monohulls, and catamarans [14] by 18%, 15%, and 12%, respectively. Some others also focused on the efficiency of installing interceptors at different locations such as near the keel or side [15] [16] [17], middle [18]. Moreover, Deng R. et al. varied the interceptor heights, deadrise angles, and simulated speeds using a computational fluid dynamic approach [19]. Several other experiments were conducted on high-speed vessels to measure resistance, trim, and center of gravity values at different interceptor speeds and heights. The results showed that the pressure under the transom increased in proportion to the size of the interceptor [20], [21]. Furthermore, Samuel et al. studied the integration of the appendage in the Aragon

\*CORRESPONDING AUTHOR | S. Samuel | ✉ [samuel@ft.undip.ac.id](mailto:samuel@ft.undip.ac.id)

2 hull design and reported a 57% drag reduction in the close-to-chine position [22]. It was also observed that the application of the v-form interceptor reduced drag by 21% at a Froude number (Fr) of 0.87 [23]. Another study found that the interceptor installed on a ship with an extended stern had a significant impact [24].

Two appendages have been combined in several studies to determine the best results. For example, the integration of the interceptor into a stern flap or trim tab performed better in reducing trim and drag [25]. Song et al. also integrated the stern flap and interceptor on the deep-vee planing hull, and the results from the experimental and numerical analyses showed an improvement in drag reduction and trim optimization [26]. Moreover, a recent study also combined interceptor with other appendages without considering the flap angle [27] and the process led to the enhancement of the running trim and motion control of planing ships across different speeds.

The observation from previous studies further indicated efforts made to improve ship drag by combining interceptors with stern flaps to achieve optimal hydrodynamic performance on the hull. For example, Mansoori et al. studied the interceptor-stern flap but failed to discuss the conversion process. The review also showed that attention had not focused on the flap angles. Therefore, this study aimed to provide quite extensive information on the aforementioned concepts by combining interceptor and stern flap to reduce the lift force at the stern of the ship during high speeds. The process involved explaining the conversion process and reviewing the flap angles to determine the different characteristics. Moreover, the Computational Fluid Dynamics (CFD) simulation results were verified using Park et al.'s experiments [28]. Numerical simulations were also conducted utilizing the Reynolds-Averaged Navier-Stokes (RANS) equation to address fluid dynamics [29] with a focus on the air-water flow around the hull and the assumption of a fixed roll and freedom in heave and pitch directions under calm water conditions.

## 2.0 METHODS

Drag performance and seakeeping were observed in the three deep-v hull shapes developed by Kim and Kim [30], followed by the design of Aragon 1 and 2 to improve stability and ship maneuverability [31]. Moreover, an identical study by Park et al. conducted experiments by installing the interceptor in Aragon 2 [28]. The data from these studies led to the adoption of a modified Aragon 2 planing hull ship model which was scaled to 1:5.33 using the specifications stated in the experiments conducted by Park et al. The parameters are presented in Table 1, while the computer-aided design (CAD) model is shown in Figure 1. Moreover, a simulation was conducted to examine the impact of the interceptor and the combined interceptor-stern flap on the performance of the planing hull, specifically during high-speed scenarios.

Table 1. Model ship dimensions

Parameter	Full Scale	Model Scale	Unit
Scale	1	5.33	-
Length Over All (LOA)	8.00	1.50	m
Length Water Line (LWL)	7.53	1.42	m
Breadth (B)	2.20	0.41	m
Draft (T)	0.42	0.08	m
Displacement ( $\Delta$ )	3000	19.78	kg
Span	300	56.28	mm
Interceptor height (i)	50	9.38	mm

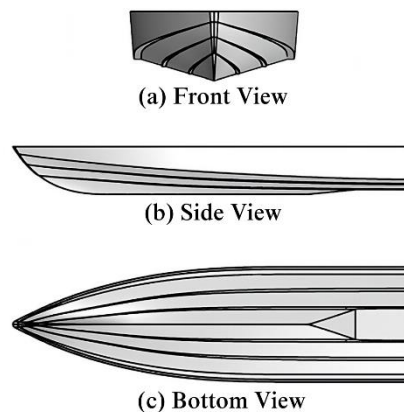


Figure 1. Planing hull shape

2.1 Research Parameters

The objective of this study was to evaluate the influence of the interceptor and integrated interceptor-stern flap (IS) on planing hull ships, particularly during high-speed conditions. The parameters considered included interceptor height ( $i$ ), stern flap chord length ( $l$ ), and integrated interceptor-stern flap span ( $s$ ) while the variables examined were ship speed and stern flap angle ( $\alpha$ ).

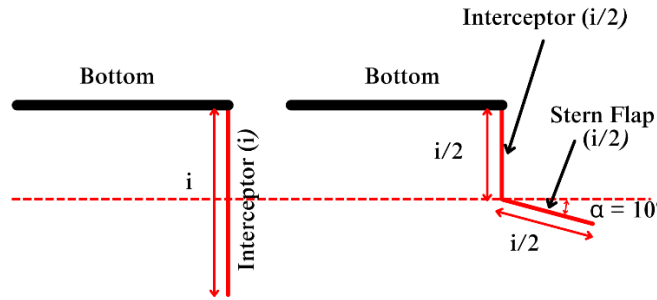


Figure 2. Integrated interceptor-stern flap concept

2.2 Model Variations

The interceptor utilized was the Humphree X300, which had a maximum stroke height ( $i$ ) of 50 mm and a span width ( $s$ ) of 300 mm on a full scale. The dimensions were subsequently adjusted to the scale ratio of the model ship. Moreover, the integrated IS was used to convert the maximum interceptor stroke to interceptor height ( $i/2$ ) and stern flap chord length ( $l$ ) as shown in Figure 2. The orientation of the stern flap angle was set at 5°, 10°, and 15° down to the horizontal axis [26]. Furthermore, the Froude numbers used as speed in this simulation were 0.29, 0.58, 0.87, 1.16, 1.45, and 1.74. All the variables used are presented in Table 2 while the parameters are described in Figure 3.

Table 2. Variation of research models

Model	$d (i + t)$ (mm)	$i$ (mm)	$t$ (mm)	$l$ (mm)	$\alpha$ (°)
Bare hull	-	-	-	-	-
Interceptor 100%	50	50	-	-	-
Integrated IS A	27.18	25	2.18	25	5
Integrated IS B	29.34	25	4.34	25	10
Integrated IS C	31.47	25	6.47	25	15

2.3 Computational Fluid Dynamics Setup

Computational Fluid Dynamics (CFD) was used to analyze fluid flow problems while the RANS equation was applied to investigate the ship resistance performance with a focus on dynamic changes of trim, sinkage, bottom pressure, and hydrodynamic forces. Moreover, the hull of the ship was simulated with or without an interceptor, and an interceptor-stern flap was applied to the transom planing vessel.

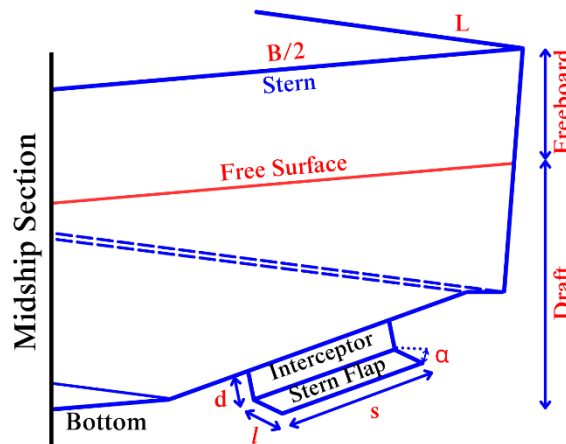


Figure 3. Dimension of integrated interceptor-stern flap

This showed that the model was simulated using CFD while the hydrodynamic aspect was based on the unsteady RANS equations which was identified as a problem-solving method designed in line with the principles of mass and momentum conservation.

$$\frac{\partial U_i}{\partial x_i} = 0 \tag{1}$$

$$\frac{\partial U_i}{\partial t} + \frac{\partial(U_i U_j)}{\partial x_j} = -\frac{1}{\rho} \frac{\partial P}{\partial x_i} + \frac{\partial}{\partial x_i} (2\nu S_{ij} - \overline{u'_i u'_j}) \tag{2}$$

Here,  $U_i$  and  $u'_i$  represent the mean and fluctuation velocity component in the direction of the Cartesian coordinate  $x_i$ ,  $\rho$  is the density,  $P$  is the mean pressure,  $S_{ij}$  is the mean strain-rate tensor and  $\nu$  is the molecular kinematic viscosity. The definition of the strain-rate tensor is:

$$S_{ij} = \frac{1}{2} \left( \frac{\partial U_i}{\partial x_j} + \frac{\partial U_j}{\partial x_i} \right) \tag{3}$$

The final term on the right-hand side of Equation 2 is identified as the Reynolds stress tensor, expressed as:

$$\tau_{ij} = \overline{u'_i u'_j} = \mu_t \left( \frac{\partial U_i}{\partial x_j} + \frac{\partial U_j}{\partial x_i} - \frac{1}{3} \frac{\partial U_k}{\partial x_k} \delta_{ij} \right) - \frac{2}{3} \rho k \delta_{ij} \tag{4}$$

The Boussinesq (eddy-viscosity) hypothesis derived from the k-ε turbulence model is articulated as follows:

$$\mu_t = \frac{1}{2} \frac{\rho \tau_{ij}}{S_{ij}} \tag{5}$$

According to the K-epsilon turbulence model, the turbulent eddy viscosity is determined by

$$\mu_t = c_\mu \rho \frac{k^2}{\varepsilon} \tag{6}$$

Below is a calculation of the turbulent kinetic energy (k) and the turbulent energy dissipation rate (ε).

$$\frac{\partial \rho k}{\partial t} + \frac{\partial \rho U_j k}{\partial x_j} = \frac{\partial}{\partial x_j} \left[ \left( \mu + \frac{\mu_t}{\sigma_k} \right) \frac{\partial k}{\partial x_j} \right] + P_k - \rho \varepsilon \tag{7}$$

$$\frac{\partial \rho \varepsilon}{\partial t} + \frac{\partial \rho U_j \varepsilon}{\partial x_j} = \frac{\partial}{\partial x_j} \left[ \left( \mu + \frac{\mu_t}{\sigma_\varepsilon} \right) \frac{\partial \varepsilon}{\partial x_j} \right] + \frac{\varepsilon}{k} (c_{\varepsilon 1} P_k - c_{\varepsilon 2} \rho \varepsilon) \tag{8}$$

### 2.4 Computational Domain

Furthermore, the computational domain was consistently based on the International Towing Tank Conference (ITTC) recommendation [32], which included a specified distance of one ship length (L) ahead of the inlet, 2.5 L from the stern to the outlet, 2 L below the keel to the bottom, 1.5 L from the middle of the ship to the top, and 1 L sides of the hull, as shown in Table 3 and Figure 4.

Table 3. The boundary conditions and computational domain

Locations	Background	Overset
Height (m)	1L from deck	0.75H from deck
	2L from keel	0.75 from keel
Length (m)	1L from forepeak	0.25 from Forepeak
	2.5L from afterpeak	0.25 from afterpeak
Breadth (m)	1.5L from symmetry	0.5B from symmetry

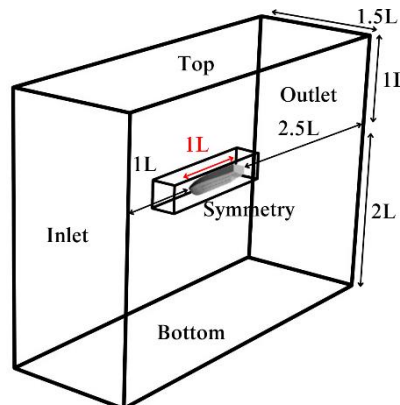


Figure 4. General view of boundary conditions

### 2.5 Boundary Condition

The boundary conditions used in the simulation are presented in Table 4, including the inlet velocity applied to describe the inlet, bottom, side, and top. Outlet boundaries were also marked sufficiently apart using pressure outlets to allow the fluid to flow fully and prevent reflection while no-slip boundary conditions were used on the body surface. Moreover, only half of the hull was considered in the CFD investigation to reduce computation time and all the typical velocities and average gradients of variables were zero in the symmetry plane.

Table 4. Boundary condition

Surface	Boundary Conditions
Inlet	Velocity inlet
Side	Velocity inlet
Symmetry	Symmetry plane
Body	Wall (no slip)
Bottom	Velocity inlet
Top	Velocity inlet
Outlet	Pressure outlet

### 2.6 Mesh Quality

The overset mesh method was used with a focus on two different meshing sections around the body, one overset as a donor and the other as an acceptor in the background. Moreover, the visualization of the mesh density produced using the method is presented in Figure 5.

Table 5. Number of elements

Mesh sizing	The quality of mesh	Number of elements
1#	Very coarse	512028
2#	Coarse	862816
3#	Medium	1219260
4#	Fine	2009497
5#	Very fine	2315182

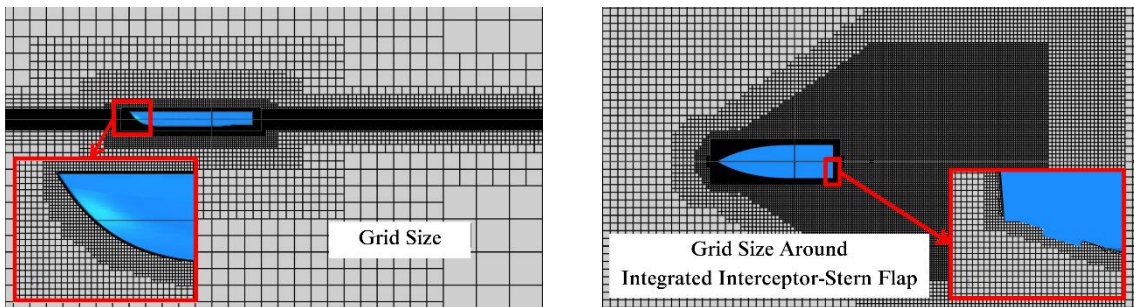


Figure 5. Mesh density visualization

The meshing process was focused on hull form and the water surface in order to produce accurate results at a relatively quick computation time. The studies related to mesh independence in selecting the correct size are presented in Table 5 and the number of total mesh elements is determined based on the previous study [33]. Furthermore, the simulation convergence ensured that the results had a correct solution where the values of errors such as resistance and trim were acceptable. The assurance of the convergence for the values acquired was accomplished to confirm the stability.

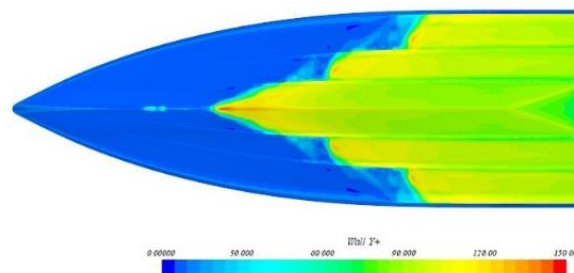


Figure 6. Dimensionless wall distance ( $y^+$ ) at Froude Number (Fr) 1.45

The study used six prism layers, each placed near the body, to record the movement of the boundary layer accurately. Moreover,  $y^+$  was targeted to ensure that the near-wall region, where viscous effects dominated, was adequately resolved in order to influence the accuracy of the results and the computational efficiency of the simulation. The dimensionless wall distance ( $y^+$ ) was also used to mitigate inaccuracies in calculations and the values were expected to be within the range of 30 to 130 to achieve accurate results [29]. However, the value could be determined using Equation 9 according to ITTC recommendations.

$$y^+ = \frac{(\rho \cdot U \cdot y)}{\mu} \tag{9}$$

Some of the variables used included  $y$  which was the thickness of the first layer,  $U$  was the friction velocity at the wall,  $\mu$  was the dynamic viscosity of the fluid. The value of  $y^+$  value on the ship was presented in Figure 6 to be at an average of 70–80 while the volume of fluid method was considered reliable for tracing the interface between air and water. Furthermore, the time step for the unsteady simulation ( $\Delta t$ ) was required to be short enough to finish the motion in an open area and was determined to average 0.008 based on the speed and length of the ship using Equation 10 in line with the recommendation of the ITTC as presented in Figure 7.

$$\Delta t_{ITTC} = 0.005 \sim 0.01 \frac{L}{V} \tag{10}$$

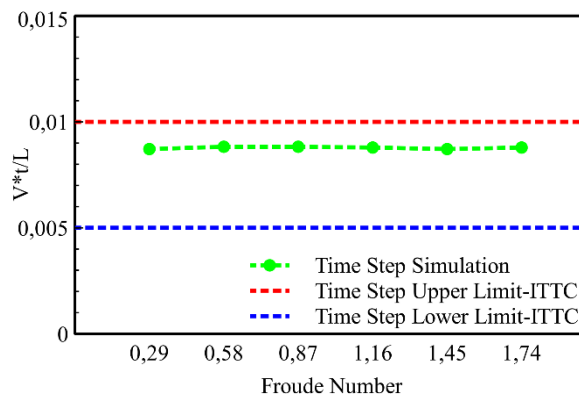


Figure 7. Time step illustration

### 2.7 Solver Settings

The solver parameters used for the simulation are listed in Table 6, which include Dynamic Fluid Body Interaction (DFBI) applied to the movement of the ship body in response to the force of the flow. The turbulence model of the simulation was realizable at  $k$ -epsilon, where  $k$  was the turbulent kinetic energy and  $\epsilon$  was the rate at which the energy dissipated. Meanwhile, a more recent development model was realizable  $k$ -epsilon which performed better in terms of dissipation rate. It is important to state that when a boundary condition such as speed or pressure changes over time or restricts motion, the concept is known as implicitly unstable. Furthermore, the pressure-velocity coupling method was achieved through the application of the SIMPLE (Semi-Implicit Method for Pressure-Linked Equations) to combine pressure and velocity.

Table 6. Solver parameters

Variable	Set-Up
Model Turbulence	Realizable $k$ - $\epsilon$
Overset Interpolation Scheme	Linear
Multiphase Model	Volume of Fluid (VOF)
Solver	3D, Unsteady, Implicit
Number of Inner Iterations	10
Pressure-Velocity Coupling	SIMPLE
Time Discretization	First Order Upwind
Motion Solver	Dynamic Fluid Body Interaction (DFBI)
Wall Treatment	Two Layer All Wall $y^+$ Treatment

### 3.0 RESULT AND DISCUSSION

#### 3.1 Mesh Independence

The computational process is usually significantly influenced by the number of cells, and this shows the need for correct values in order to provide accurate results relatively quickly. Therefore, the independence mesh was required to obtain convergent results and this was achieved by comparing the resistance, trim, and heave values to the total number of cells, as shown in Figure 8. The simulation was later performed on five grid variations at Fr 1.45 while the resistance was visualized in non-dimensional  $R/\Delta$  units on the y-axis. Moreover, the trim was in degrees, and the heave was in units with a non-dimensional rise in CG/draft units. The components on the x-axis were the variations in the number of cells of different qualities.

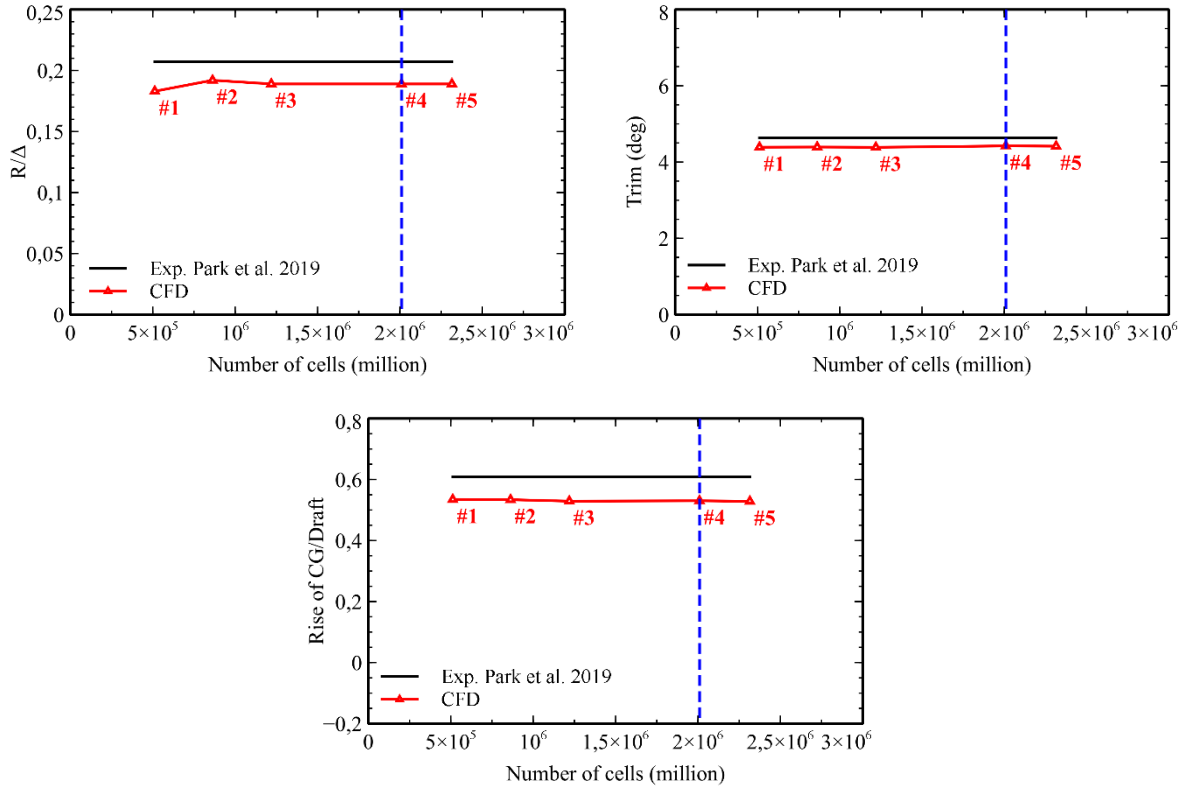


Figure 8. Mesh independence study

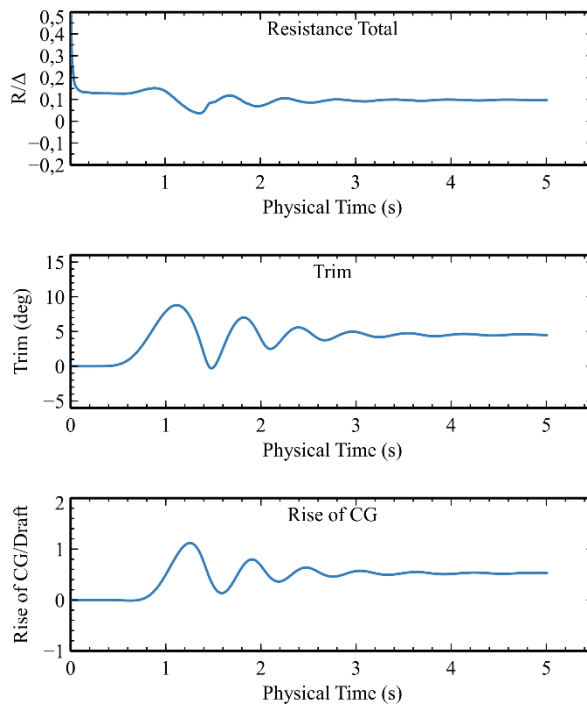


Figure 9. Mesh convergence trends for drag, trim, and heave bare hull models at Fr 1.45

The results presented in the resistance graph showed that the mesh converged on meshes #4 and #5 with good accuracy. However, mesh 5 required a longer computation time than mesh #4 due to the presence of more cell numbers. This led to the selection of mesh #4 for the simulation, featuring a total of 2 million cells, and the computational resistance error was 8.59%, the computational trim error was 4.57%, and the heave error was 12.84% compared to the experiment. The result was considered satisfactory, specifically due to the complexity of the planing ship simulation, as observed in the minimization of computation time and maintenance of convergence. Furthermore, the ship resistance, trim, and heave values generated from the simulation model were evaluated based on the time to demonstrate the similarity as presented in Figure 9. It was observed that all the data started converging after 4 seconds of the simulation process.

### 3.2 Model Validation

The ship resistance, trim, and heave values were validated based on the experimental results in Figure 10, and those from the simulation were found to be lower. The difference was probably due to the difficulty associated with the measurement process during the experiment. The pattern between the two methods has always been consistent, leading to the declaration of the results from numerical computations. Some differences were also identified in the calculation errors due to difficulties in modeling an object in numerical computation based on the conditions used in experimenting with towing tanks. A similar trend has been reported by Hosseini et al. [34] and Utomo et al. [21] during the application of CFD calculations to planing ships, presenting an error of 4.63% to 9.97% in predicting ship resistance compared to the experimental results.

The error value produced in determining the resistance at bare hull conditions was 7.76% at Fr 1.45 and the average was 9.19% for all speed variations. The application of the interceptor changed the resistance error value to 11.21% and 11.23%, respectively. This led to the declaration that the model was developed as valid based on the production of appropriate error values and the similarity in the patterns between numerical computations and experimental results.

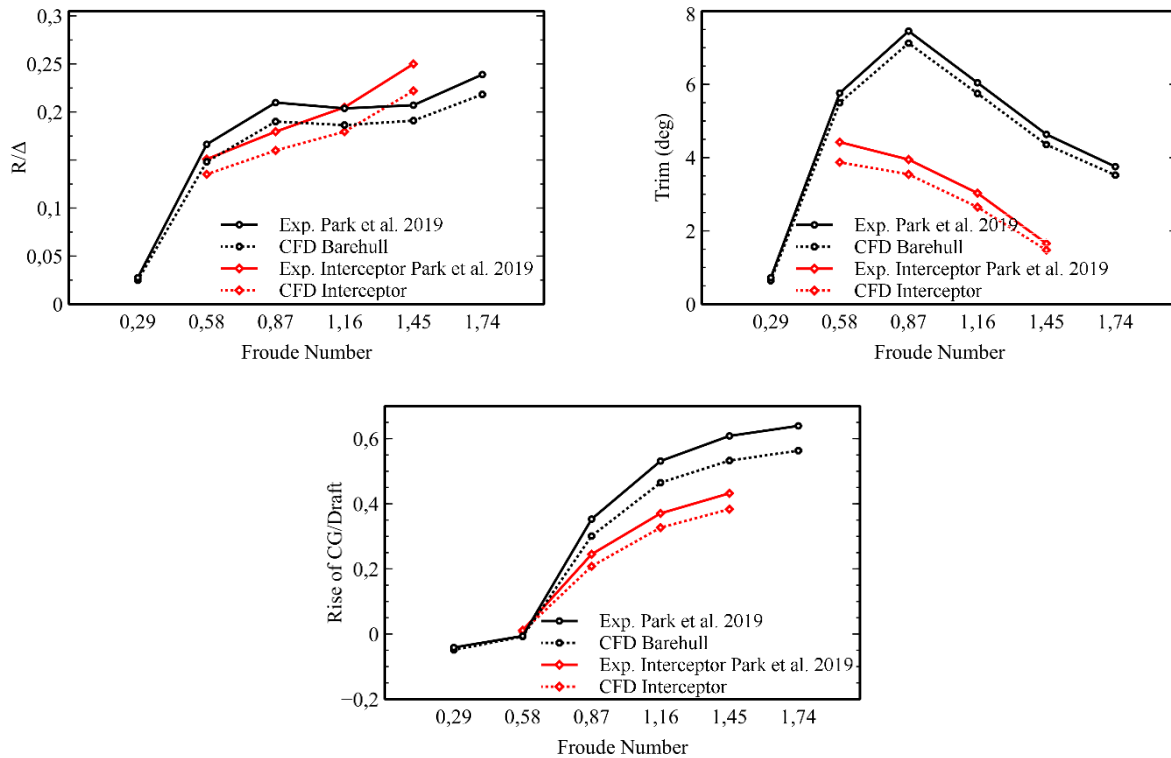


Figure 10. Ship resistance, trim, and heave between CFD and experiments

### 3.3 Interceptor Effect

The maximum interceptor height ( $d$ ) was determined in all the simulations by assessing the boundary layer thickness ( $h$ ). This was in line with the explanation of the previous study by Mansoori and Fernandes [25] that the thickness of the boundary layer was the main key to determining the height of the interceptor. Moreover, the interceptor produced a pressure distribution near the stern, which consequently led to the development of the moment ( $M_2$ ) in Figure 11, which was in contrast to the trim moment ( $M_1$ ) in Figure 11, which was caused by pressure. It was also observed that the interceptor was able to generate additional lift and drag. The interceptor was considered optimal when  $M_2 = M_1$  depending on the height ( $d$ ) and boundary layer thickness ( $h$ ) or  $d/h = 0.6$ . The criterion also showed that  $M_2 < M_1$  or  $d/h$  less than 0.6 was adjudged to be a weak condition. Meanwhile, the condition was considered unfit when  $M_2 > M_1$ , the lift was more than just a drag to make a negative trim, or  $d/h$  was greater than 0.6 due to the ability to increase the total resistance and instability of the ship [25]. The result further showed that an increase in ship speed led to a reduction in the thickness of the boundary layer, as shown in Figure 12.

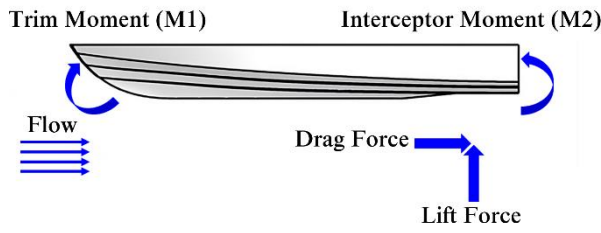


Figure 11. The force acting on the ship using the interceptor

The effect of drag, heave, trim, and lift forces on an interceptor mounted on the transom of the ship is presented in Figure 13, in addition to the change in the thickness of the boundary layer at several points in non-dimensional  $d/h$  units. It has been stated that the interceptor offered weak efficiency in reducing drag and trim when the  $d/h$  ratio was less than 0.6. However, the performance was observed to be better than the current state of the ship but became inefficient when  $d/h$  exceeded 0.6 and generated a powerful and dangerous moment, which could cause the trim to become negative. Under more adverse conditions, the trim moment can capsize the ship and this is similar to the report of Mansoori and Fernandes [25] concerning the relationship between interceptor height and the boundary layer thickness.

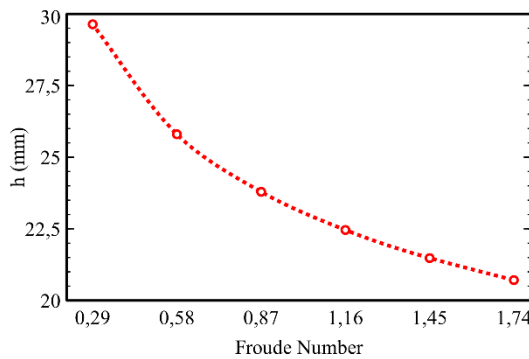


Figure 12. The boundary layer thickness at each ship speed

The addition of the interceptor provided a significant reduction in drag at low Fr (0.29–1.16) but generated more substantial drag at high Fr (1.45–1.78). The most significant decrease in resistance was recorded to be 15.85% at Fr 0.87 while the trim value reduced at all variations of speed. However, the trim became more extreme, approaching zero, at a high Fr and had the potential to induce negative values on the ship, leading to non-recommendation of the interceptor. An increase in the speed of the ship without the interceptor led to an increment in the lift force. However, the value continued to increase after the interceptor was installed along with the Fr, and the highest was recorded to be 4.01% at Fr 1.45.

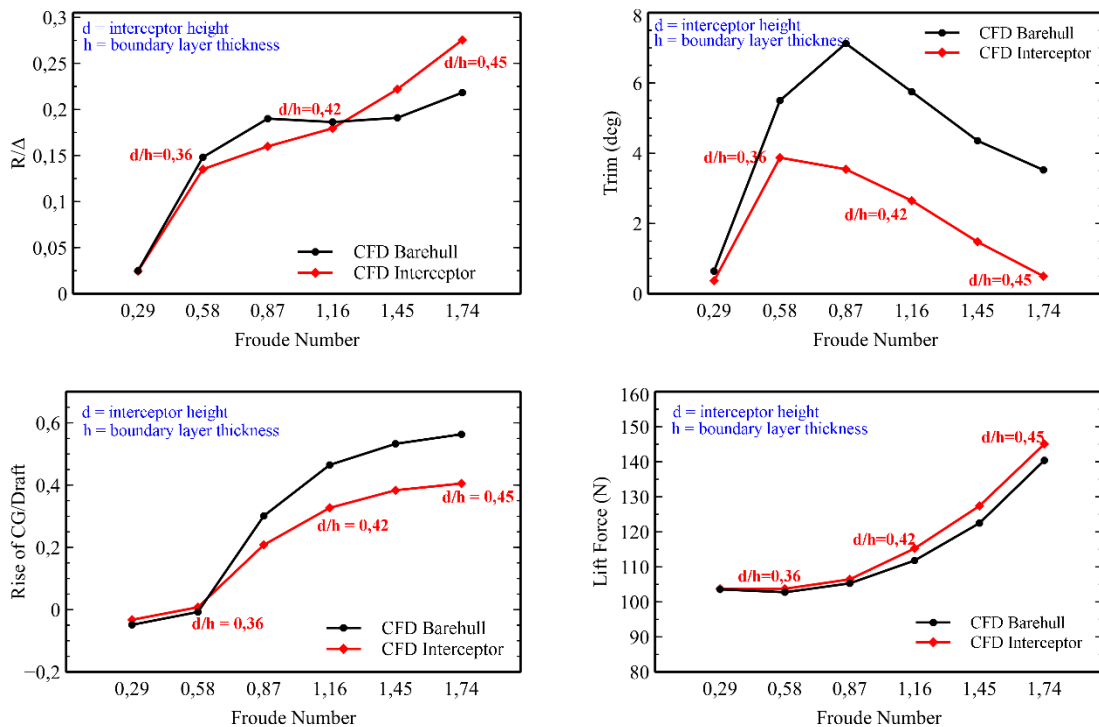


Figure 13. Relationship of the ratio of boundary layer thickness vs. interceptor

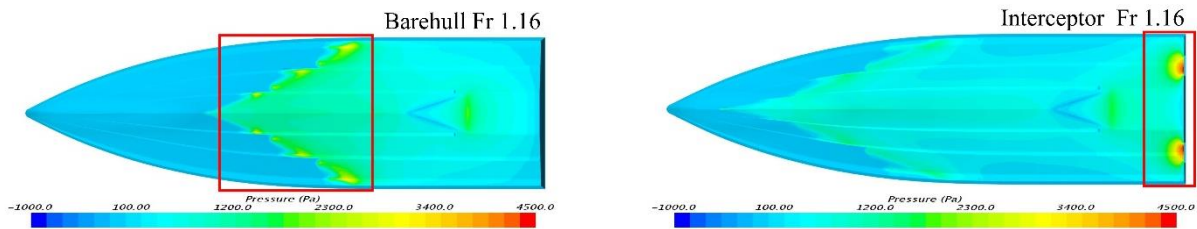


Figure 14. Bare hull and interceptor pressure distribution

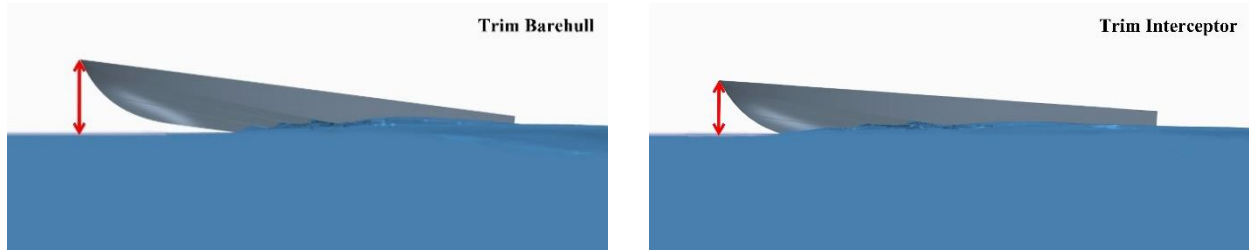


Figure 15. The interceptor effect at Fr 0.87

The pressure on a ship without the interceptor was concentrated in the midship area as presented in Figure 14, causing the moment at the bow to be greater when compared to the stern with a subsequent effect on the trim as shown in Figure 15. The optimal interceptor was determined when the moment was almost the same as the trim moment caused by water pressure. This was confirmed by Mansoori and Fernandes' report that an increase in the height of the interceptor led to negative trim at high speeds.

### 3.4 Integrated Interceptor-Stern Flap Effect

The interceptor produced quite a good lift and drag reduction when  $d/h$  was close to 0.6 but the resistance increased significantly when the value was greater. The height of the interceptor was required to be lowered to resolve the problem even though the process could reduce the lift force. Therefore, this study was focused on solving the problem of using the interceptor on planing ships without significant loss of lift by adding the stern flap, specifically at high speeds. The system was converted into two parts, including the interceptor and stern flap. The chord length of the stern flap ( $l$ ) was equal to half of the interceptor's height at different flap angles. The previous discussion confirmed the importance of the interceptor size and the need to consider the thickness of the boundary layer of the transom section. Therefore, the total height ( $d$ ) used was calculated using Equations 11 and 12, where  $d$  was the sum of the height of the interceptor ( $i$ ) and the stern flap ( $t$ ) as shown in Figure 16.

$$d = i + t \tag{11}$$

$$t = l \times \sin \alpha \tag{12}$$

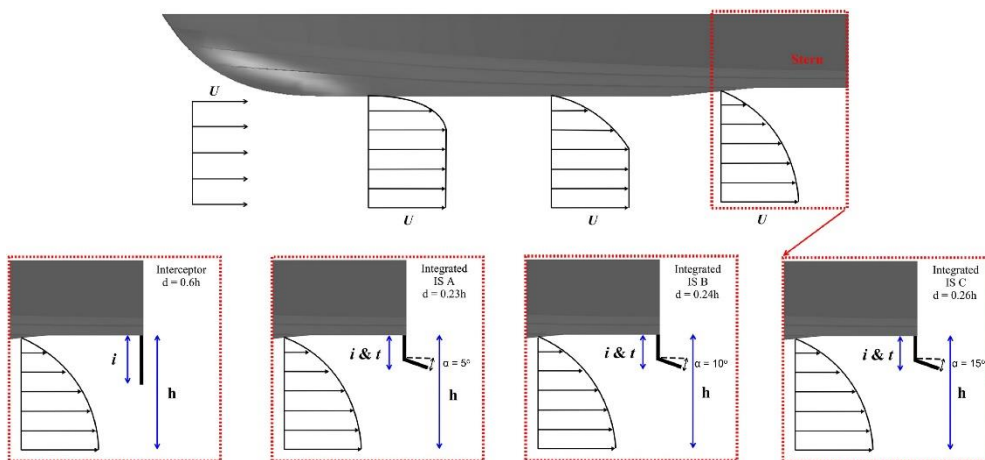


Figure 16. Sketch of the boundary layer at the bottom of the vessel

The values of the resistance, trim, heave, and lift forces were considered after the conversion process as presented in Figure 17. The results showed significant changes in the parameters of the ship at high speeds, specifically the resistance, with the application of integrated IS reported to have better performance in almost all the variables. This was observed in the superior resistance performance recorded at Fr 1.45 compared to the ships without flaps or with only interceptors. The

trend was further reported in different flap angles where drag was reduced effectively at Fr 0.29–1.45 while a slight increase was found at Fr 1.74 as the angle increased. The understanding of the flap angle ( $\alpha$ ) is necessary to determine the effect of the stern flap as discussed in earlier studies and the value is required not to be more than the stall angle because the lift produced by the stern flap can reduce when the value is greater than  $12^\circ$  [25]. Furthermore, the best resistance reduction was found with integrated IS flap A at an average of 6.49% while the highest was 18.34% in flap C at Fr 0.87. This showed that the acceleration of the ship with the developed integrated IS could reduce the trim value by 17.5 to 43.86% but had the capacity to increase the value through the application of a larger flap angle. The results further showed that all variations of the integrated IS with different angles were able to reduce the trim of the bare hull. The ships designed using the model can also reduce heave value and increase speed. The pattern observed in the trim was identified in the flap effect which increased with the flap angle value, but the integrated IS was able to reduce the heave of the bare hull.

The lift force increased with speed on all variations of the integrated IS, which led to the reduction of the ship's wet surface and, subsequently, the drag, specifically at high Fr. The highest lift force value was found to be 5.64% at Fr 1.74 in flap C and this was in line with the initial aim of the study which required reducing the interceptor height and lift force to avoid negative trim. Meanwhile, the model did not significantly eliminate the lift force value and could reduce the resistance value.

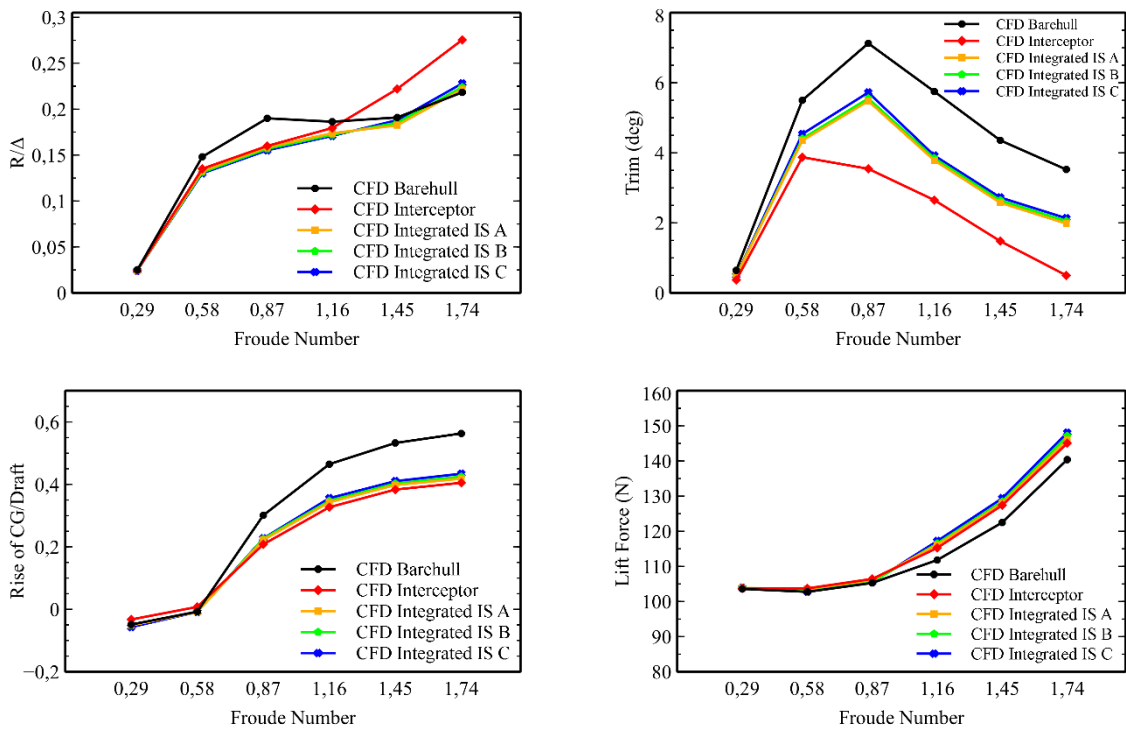


Figure 17. Effect of interceptor installation on resistance, trim, heave, and lift force

The changes in pressure due to the usage of interceptor and integrated IS are identified in Figure 18. The results showed the distribution of higher pressure by the interceptor on the hull in front as presented in Figure 18a. The shifting of the interceptor to a higher position changed the concentration of the pressure to the stern of the ship but at a lower magnitude as presented in Figure 18b because only half of the height was used.

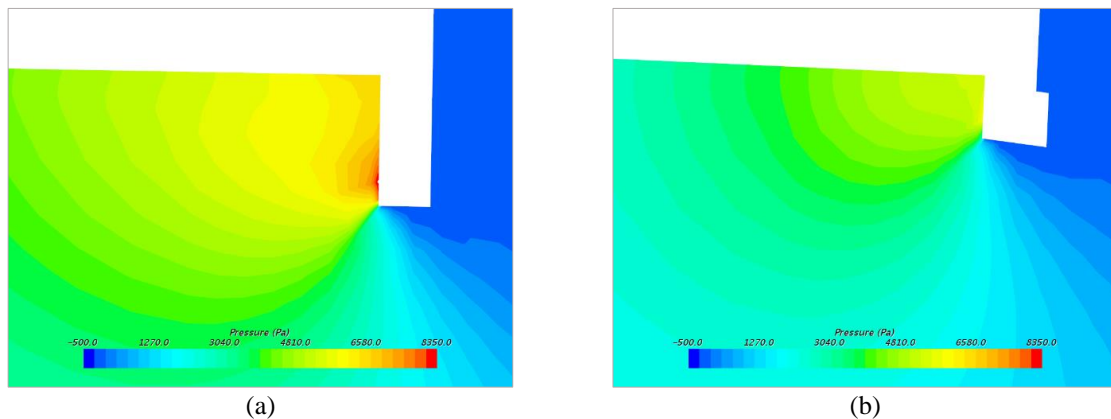


Figure 18. The high-pressure area on interceptor (a) and integrated interceptor-stern flap (b) at Fr 1.45

Figure 19 shows the wave pattern captured behind the transom on the bare hull through the application of both interceptor and integrated IS at Fr 1.45. The separated flow converged downstream of the stern, leading to the development of the rooster tail. Moreover, the region of fluid flow behind the stern included a hull hollow, rooster tail, and divergent wave systems caused by breaking which could be reduced through the introduction of interceptor and integrated IS into the hull of the ship, leading to a decrease in drag. The working process of the interceptor to reduce the height of the rooster tail and the area covered by breaking divergent waves to minimize energy losses in the ship near the field is also presented in the figure.

The results further showed that the flap angle on the interceptor stern flap influenced the thickness of the boundary layer. This was observed from the fact that the increase in the angle value led to a rise in the  $d/h$  value at each speed. The  $d/h$  values for a ship with an interceptor, integrated IS-A, and bare hull are compared in Figure 20. The resistance of the ship was found to improve as the  $d/h$  ratio reduced due to the decrease in the boundary layer thickness at higher speed. This information is very important for operators despite the possibility of controlling the height of the interceptor because the negative trim associated with an increase in speed can cause an imbalance in the bow, thereby making the ship capsize. The observation from the study showed that IS-A with a flap angle of  $5^\circ$  provided better hydrodynamic performance at almost all speeds by having a lower resistance value. This was due to the reduction in the wet surface of the ship caused by the decrease in trim and an increase in lift force. Furthermore, the results showed a decrease of 1-16% in drag and 20-43% in trim due to the implementation of integrated IS-A at a flap angle of  $5^\circ$  and different Fr when compared to a bare hull as presented in Figure 21.

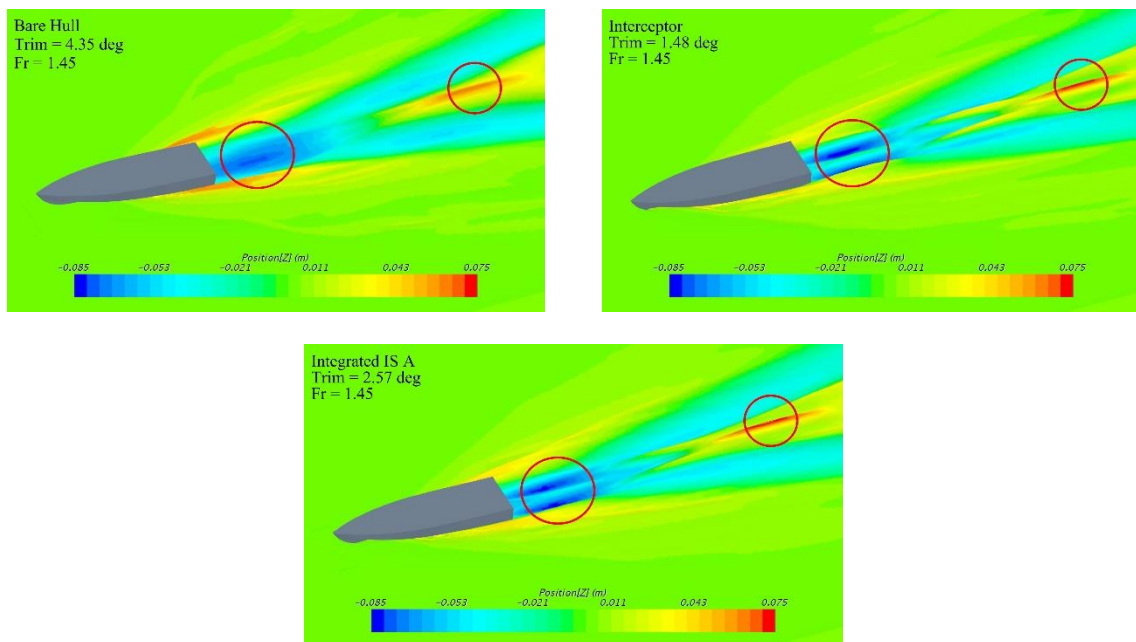


Figure 19. Comparison of wave pattern on bare hull, interceptor dan integrated IS A at Fr 1.45

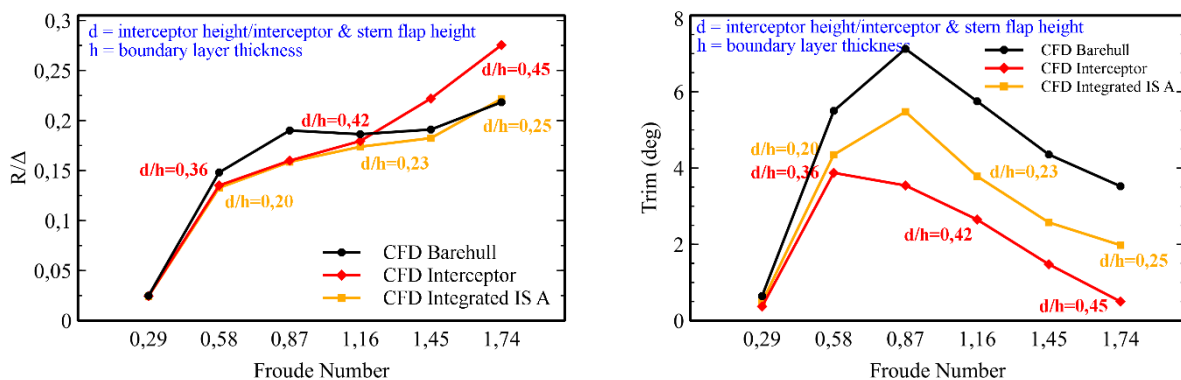


Figure 20. Comparison of trim and resistance of bare hull, interceptor, and integrated IS A

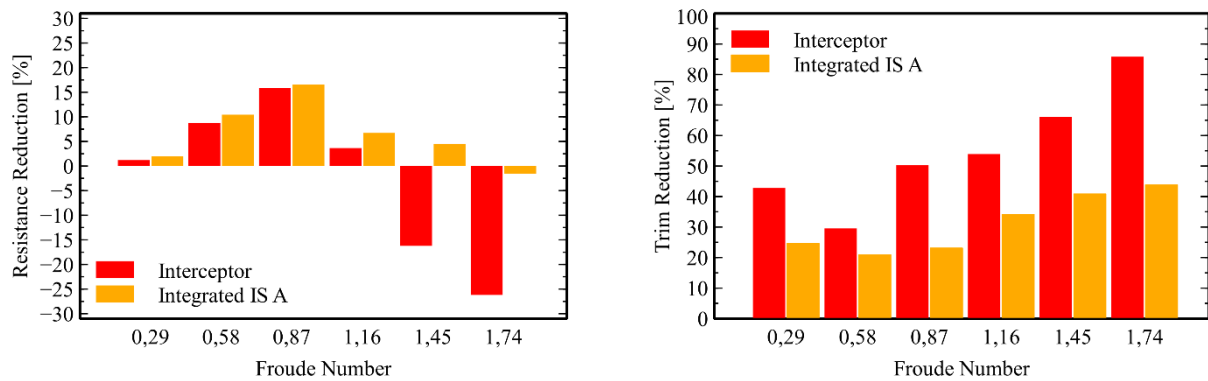


Figure 21. Percentage of drag and trim reduction between the interceptor and the integrated IS A

#### 4.0 CONCLUSIONS

In conclusion, the objective of this study was to address the challenge associated with using the interceptor at high speeds by reducing the height and adding the stern flap. Numerical simulations were conducted using the RANS equation on the planing ship at different configurations, including without the interceptor, with the interceptor, and with the integrated interceptor-stern flap at different angles. The drag and trim model developed was found to be valid based on the previous experiments conducted by Park et al. Moreover, the number of meshes was reported to be important in improving the accuracy of numerical simulations which led to the selection of the most appropriate value. The impacts of the configurations were determined on the drag, trim, heave, and lift force of the ship, and the summary of the results is presented as follows:

- The interceptor reduced resistance by 1–16% at Fr 0.29–1.16 compared to a bare hull but increased drag at high speeds of Fr 1.45 and 1.74. The decrease in resistance was associated with the lift generated by the pressure on the ship due to the presence of the interceptor while the increase at high speed was based on the moment developed which was related to the  $d/h$  ratio. The inclusion of the interceptor also reduced the trim by 29–85% at all the Froude numbers, and this showed its suitability as a trim controller. Meanwhile, trim height increased extremely, approaching zero and potentially leading to a negative value, at high Froude numbers. The process led to the non-recommendation of the interceptor at high Froude numbers.
- The application of different flap angles on the stern flaps integrated into the interceptor was effective in reducing drag and trim. The integrated IS-A with a  $5^\circ$  flap had the best performance in reducing resistance ranging from 2% to 17% with an average of 6.5% across all Froude numbers compared to a bare hull. It was also able to reduce the trim by 17–43% compared to the empty hull in all variations at different Froude numbers. The trend showed the ability of the integrated IS to function effectively as a trim controller without producing negative values at high speeds. This led to the consideration of the interceptor height as an important parameter to improve the performance of ships.

#### 5.0 ACKNOWLEDGEMENT

The author would like to thank all members of the Hydrodynamics Laboratory, Department of Naval Architecture, Faculty of Engineering, Diponegoro University Semarang for their support in conducting this research.

#### 6.0 REFERENCES

- [1] A. Z. Ashkezari and M. Moradi, "Three-dimensional simulation and evaluation of the hydrodynamic effects of stern wedges on the performance and stability of high-speed planing monohull craft," *Applied Ocean Research.*, vol. 110, p. 102585, 2021.
- [2] S. Samuel, P. Manik, R. Praja, T. Tuswan, P. Paryanto, M. Djaeni, "Numerical investigation of extended stern to reduce resistance of planing hull," *Transactions on Maritime Science*, vol. 13, no. 1, 2023.
- [3] J. Zou, S. Lu, Y. Jiang, H. Sun, and Z. Li, "Experimental and numerical research on the influence of stern flap mounting angle on double-stepped planing hull hydrodynamic performance," *Journal of Marine Science and Engineering*, vol. 7, no. 10, pp. 1–25, 2019.
- [4] C. Çelik, D. B. Danişman, S. Khan, and P. Kaklis, "A reduced order data-driven method for resistance prediction and shape optimization of hull vane," *Ocean Engineering*, vol. 235, p. 109406, 2021.
- [5] M. Mansoori and A. C. Fernandes, "Hydrodynamics of the interceptor on a 2-D flat plate by CFD and experiments," *Journal of Hydrodynamics*, vol. 27, no. 6, pp. 919–933, 2015.
- [6] K. wei Song, C. yu Guo, J. Gong, P. Li, and L. zhou Wang, "Influence of interceptors, stern flaps, and their combinations on the hydrodynamic performance of a deep-vee ship," *Ocean Engineering*, vol. 170, pp. 306–320, 2018.

- [7] A. Maki, J. Arai, T. Tsutsumoto, K. Suzuki, and Y. Miyauchi, "Fundamental research on resistance reduction of surface combatants due to stern flaps," *Journal of Marine Science and Technology*, vol. 21, no. 2, pp. 344–358, 2016.
- [8] K. wei Song, C. yu Guo, C. Wang, C. Sun, P. Li, and W. Wang, "Numerical analysis of the effects of stern flaps on ship resistance and propulsion performance," *Ocean Engineering*, vol. 193, no. 106621, pp. 1–19, 2019.
- [9] P. Zhou, J. Fu, J. Zhu, and H. Xu, "Model test study on parameter optimization of stern flaps of series displacement ships," *IOP Conference Series: Earth and Environmental Science*, 2019, vol. 219, no. 1, p. 012030.
- [10] H. Ghassemi, M. Mansouri, and S. Zaferanlouei, "Interceptor hydrodynamic analysis for handling trim control problems in the high-speed crafts," *Proceedings of the Institution of Mechanical Engineers, Part C: Journal of Mechanical Engineering Science*, vol. 225, no. 11, pp. 2597–2618, 2011.
- [11] M. Mansoori and A. C. Fernandes, "Hydrodynamics of the interceptor analysis via both ultrareduced model test and dynamic computational fluid dynamics simulation," *Journal of Offshore Mechanics and Arctic Engineering*, vol. 139, no. 2, pp. 021101, 2016.
- [12] M. Mansoori and A. C. Fernandes, "The interceptor hydrodynamic analysis for controlling the porpoising instability in high speed crafts," *Applied Ocean Research*, vol. 57, pp. 40–51, 2016.
- [13] A. H. Day and C. Cooper, "An experimental study of interceptors for drag reduction on high-performance sailing yachts," *Ocean Engineering*, vol. 38, pp. 983–994, 2011.
- [14] M. H. Karimi, M. S. Seif, and M. Abbaspoor, "An experimental study of interceptor's effectiveness on hydrodynamic performance of high-speed planing crafts," *Polish Maritime Research*, vol. 20, no. 2, pp. 21–29, 2013.
- [15] A. M. F. Putra and H. Suzuki, "Experimental and numerical study on the high-speed ship hydrodynamics influenced by an interceptor with varied angle of attack," *International Journal of Naval Architecture and Ocean Engineering*, vol. 16, no. 100566, pp. 1–15, 2024.
- [16] O. S. Sahin, E. Kahramanoglu, and F. Cakici, "Numerical evaluation on the effects of interceptor layout and blade heights for a prismatic planing hull," *Applied Ocean Research*, vol. 127, no. 103302, pp. 1–14, 2022.
- [17] A. G. Avci and B. Barlas, "An experimental investigation of interceptors for a high-speed hull," *International Journal of Naval Architecture and Ocean Engineering*, vol. 11, no. 1, pp. 256–273, 2019.
- [18] S. Samuel, A. Setiawan, E. S. Hadi, M. Iqbal, and P. Manik, "Study of middle interceptor implementation on patrol boat," in *Proceedings of 7th International Conference on Industrial, Mechanical, Electrical and Chemical Engineering*, vol. 2674, 2023.
- [19] R. Deng, S. Y. Chen, T. C. Wu, F. Q. Luo, D. P. Jiang, and Y. L. Li, "Investigation on the influence induced by interceptor on the viscous flow field of deep-Vee vessel," *Ocean Engineering*, vol. 196, no. 106735, pp. 1–18, 2020.
- [20] W. Seok, S. Y. Park, and S. H. Rhee, "An experimental study on the stern bottom pressure distribution of a high-speed planing vessel with and without interceptors," *International Journal of Naval Architecture and Ocean Engineering*, vol. 12, pp. 691–698, 2020.
- [21] B. Utomo, S. S. S. Yulianti, G. Rindo, M. Iqbal, and A. Fathuddiin, "CFD simulation verification processes at planing hulls using an interceptor," *Jurnal Ilmu Pengetahuan dan Teknologi Kelautan*, vol. 19, no. 3, pp. 141–150, 2022.
- [22] S. Samuel, O. Mursid, S. Yulianti, Kiryanto, and M. Iqbal, "Evaluation of interceptor design to reduce drag on planing hull," *Brodogradnja*, vol. 73, no. 3, pp. 93–110, 2022.
- [23] S. Samuel, S. Yulianti, P. Manik, and A. Fathuddiin, "A study of interceptor performance for deep-v planing hull," in *IOP Conference Series: Earth and Environmental Science*, vol. 1081, no. 1, p. 012004, 2022.
- [24] S. Samuel, R. K. Praja, D. Chrismianto, M. L. Hakim, A. Fitriadhy, and A. Bahatmaka, "Advancing interceptor design: analyzing the impact of extended stern form on Deep-V planing hulls," *CFD Letters*, vol. 16, no. 5, pp. 59–77, 2024.
- [25] M. Mansoori and A. C. Fernandes, "Interceptor and trim tab combination to prevent interceptor's unfit effects," *Ocean Engineering*, vol. 134, pp. 140–156, 2017.
- [26] K. W. Song, C. Y. Guo, J. Gong, P. Li, and L. Z. Wang, "Influence of interceptors, stern flaps and their combinations on the hydrodynamic performance of a deep vee ship," *Ocean Engineering*, vol. 170, pp. 306–320, 2018.
- [27] S. Samuel, S. Yulianti, P. Manik, A. Trimulyono, A. Firdhaus, Tuswan et al., "Numerical research on the influence of interceptor flaps on the planing hydrodynamic performance," *Nase More*, vol. 70, no. 4, pp. 219–227, 2023.
- [28] J. Y. Park, H. Cho, J. Lee, H. Choi, J. Woo, S. Kim et al., "An experimental study on vertical motion control of a high-speed planing vessel using a controllable interceptor in waves," *Ocean Engineering*, vol. 173, pp. 841–850, 2019.

- [29] J. Suneela, P. Krishnankutty, and V. A. Subramanian, "Hydrodynamic performance of planing craft with interceptor-flap hybrid combination," *Journal of Ocean Engineering and Marine Energy*, vol. 7, no. 4, pp. 421-438, 2021.
- [30] D. J. Kim, S. Y. Kim, Y. J. You, K. P. Rhee, S. H. Kim, and Y. G. Kim, "Design of high-speed planing hulls for the improvement of resistance and seakeeping performance," *International Journal of Naval Architecture and Ocean Engineering*, vol. 5, no. 1, pp. 161-177, 2013.
- [31] D. J. Kim and S. Y. Kim, "Turning characteristics of waterjet propelled planing boat at semi-planing speeds," *Ocean Engineering*, vol. 143, pp. 24–33, 2017.
- [32] International Towing Tank Conference, "Recommended Procedures and Guidelines: Practical Guidelines for Ship CFD," *Recommended Procedures and Guidelines*, pp. 1–18, 2011.
- [33] A. Fitriadhy, S. A. Azmi, N. Aqila Mansor, and N. Adlina Aldin, "Computational fluid dynamics investigation on total resistance coefficient of a high-speed 'deep-V' catamaran in shallow water," *International Journal of Automotive and Mechanical Engineering*, vol. 14, no. 2, pp. 4369–4382, 2017.
- [34] A. Hosseini, S. Tavakoli, A. Dashtimanesh, P. K. Sahoo, and M. Kõrgesaar, "Performance prediction of a hard-chine planing hull by employing different CFD models," *Journal of Marine Science and Engineering*, vol. 9, no. 5, 2021.